mathematics

MDPI

Article

Homological Landscape of Human Brain Functional Sub-Circuits

Duy Duong-Tran [1,2,†], Ralph Kaufmann [3,†], Jiong Chen [1,4,†], Xuan Wang [5], Sumita Garai [1], Frederick H. Xu [1], Jingxuan Bao [1], Enrico Amico [6,7], Alan D. Kaplan [8], Giovanni Petri [9,10,11], Joaquin Goni [12,13,14], Yize Zhao [15] and Li Shen [1,*]

1 Department of Biostatistics, Epidemiology and Informatics, Perelman School of Medicine, University of Pennsylvania, Philadelphia, PA 19104, USA; duongtra@usna.edu (D.D.-T.); jiongc@seas.upenn.edu (J.C.); sumita.garai@pennmedicine.upenn.edu (S.G.); fredxu@seas.upenn.edu (F.H.X.); jingxuan.bao@pennmedicine.upenn.edu (J.B.)
2 Department of Mathematics, United States Naval Academy, Annapolis, MD 21402, USA
3 Department of Mathematics, Purdue University, West Lafayette, IN 47907, USA; rkaufman@math.purdue.edu
4 Department of Bioengineering, School of Engineering and Applied Science, University of Pennsylvania, Pennsylvania, PA 19104, USA
5 Department of Electrical and Computer Engineering, George Mason University, Fairfax, VA 22030, USA; xwang64@gmu.edu
6 Neuro-X Institute, Swiss Federal Institute of Technology Lausanne, 1015 Geneva, Switzerland
7 Department of Radiology and Medical Informatics, University of Geneva, 1211 Geneva, Switzerland
8 Computational Engineering Division, Lawrence Livermore National Laboratory, Livermore, CA 94550, USA; kaplan7@llnl.gov
9 CENTAI Institute, 10138 Torino, Italy; giovanni.petri@nulondon.ac.uk
10 NPLab, Network Science Institute, Northeastern University London, London E1W 1LP, UK
11 Networks Unit, IMT Lucca Institute, 55100 Lucca, Italy
12 Purdue Institute for Integrative Neuroscience, Purdue University, West Lafayette, IN 47907, USA; jgonicor@purdue.edu
13 School of Industrial Engineering, Purdue University, West Lafayette, IN 47907, USA
14 Weldon School of Biomedical Engineering, Purdue University, West Lafayette, IN 47907, USA
15 School of Public Health, Yale University, New Heaven, CT 06520, USA; yize.zhao@yale.edu
* Correspondence: li.shen@pennmedicine.upenn.edu
† These authors contributed equally to this work.

check for updates

Citation: Duong-Tran, D.; Kaufmann, R.; Chen, J.; Wang, X.; Garai, S.; Xu, F.H.; Bao, J.; Amico, E.; Kaplan, A.D.; Petri, G.; et al. Homological Landscape of Human Brain Functional Sub-Circuits. *Mathematics* **2024**, *12*, 455. https://doi.org/10.3390/math12030455

Received: 25 December 2023
Revised: 27 January 2024
Accepted: 29 January 2024
Published: 31 January 2024

Copyright: © 2024 by the authors. Licensee MDPI, Basel, Switzerland. This article is an open access article distributed under the terms and conditions of the Creative Commons Attribution (CC BY) license (https://creativecommons.org/licenses/by/4.0/).

Abstract: Human whole-brain functional connectivity networks have been shown to exhibit both local/quasilocal (e.g., a set of functional sub-circuits induced by node or edge attributes) and non-local (e.g., higher-order functional coordination patterns) properties. Nonetheless, the non-local properties of topological strata induced by local/quasilocal functional sub-circuits have yet to be addressed. To that end, we proposed a homological formalism that enables the quantification of higher-order characteristics of human brain functional sub-circuits. Our results indicate that each homological order uniquely unravels diverse, complementary properties of human brain functional sub-circuits. Noticeably, the H_1 homological distance between rest and motor task was observed at both the whole-brain and sub-circuit consolidated levels, which suggested the self-similarity property of human brain functional connectivity unraveled by a homological kernel. Furthermore, at the whole-brain level, the rest–task differentiation was found to be most prominent between rest and different tasks at different homological orders: (i) Emotion task (H_0), (ii) Motor task (H_1), and (iii) Working memory task (H_2). At the functional sub-circuit level, the rest–task functional dichotomy of the default mode network is found to be mostly prominent at the first and second homological scaffolds. Also at such scale, we found that the limbic network plays a significant role in homological reconfiguration across both the task and subject domains, which paves the way for subsequent investigations on the complex neuro-physiological role of such network. From a wider perspective, our formalism can be applied, beyond brain connectomics, to study the non-localized coordination patterns of localized structures stretching across complex network fibers.

Keywords: functional sub-circuit; functional networks; homological kernel; topological data analysis

MSC: 55N31

1. Introduction

Network science sheds light on complex phenomena—from fake news spreading mechanisms in a social network to the natural equilibrium in large-scale ecosystems with competing species' interactions. Graphs (networks), despite their convenience and power to unravel many important phenomena from social and financial to biological networks, lack the comprehensive ability to describe higher-order dynamics of complex systems [1]. Indeed, many real-world systems, although they can be described using diatic relation (edges), have indeed polyadic functionality [2,3]. Prior studies have strongly suggested the critical role of higher-order interactions in terms of explaining complex intertwined dynamics such as phase transitions of emergent phenomena in networked systems [1]. For instance, higher-order effects which emerge from the neuronal population are shown to be significant in both statistical, topological, and other domains [2,4–6]. Higher-order interactions, as formalized by hyperedges (in hypergraphs) or simplicial complexes (in homology), have shown to unravel many complementary functions, compared to node-/edge-based investigations [1].

The human brain is a complex system exhibiting a multi-scale property wherein interactions among its finest elements (e.g., neurons) orchestrate emergent phenomena (e.g., cognition, consciousness [7]). Besides exerting a hierarchical cytoarchitecture, human brain functional organizations also display "modular" characteristics—also known as hierarchical modularity [8]. Bullmore and Sporns [9] were among the first investigators noting that whole-brain functional connectivity can effectively be characterized into (functional) modules whose elements (e.g., nodes/vertices in a functional connectome (FC)) are contributed to by different distributed areas across the cortex. Specifically, the human brain can be decomposed into specialized, yet highly interactive functional modules [7,10] (or equivalently, communities in complex networks, see [11–13] among others). The modular setting of the human brain into distinctive functional sub-circuits allows its function to adapt flexibly to diverse cognitive requirements [14,15]. Moreover, functional modularity can also explain human brain complexity [7], cognitive reconfiguration [14], rest–task divergence [16], among other functionalities.

In 2011, the concept of intrinsic functional connectivity Magnetic Resonance Imaging (fcMRI) network (also known as functional sub-circuits, functional network (FN) or resting-state networks (RSNs)) was put forth by Yeo and colleagues [17]. FNs are essentially parallel interdigitated sub-circuits in which each cortical lobe may contain multiple regions belonging to one or more FNs. An a priori set of FNs (or equivalently, functional sub-circuits) elucidates different executive functions of human brain in healthy, neurodegenerative disease, or developmental conditions [18]. Mathematically, an a priori identification of FNs is a partition of the whole-brain functional connectivity, which results in a functional atlas (e.g., a guidance to which brain region(s) belong to which functional sub-circuit(s)). Such partition can be used as a baseline reference to investigate physiological, functional, and individual differences of (i) the same FN across different cognitive conditions [14] or (ii) different FNs across the same task (e.g., fMRI). Specifically, the mapping of an a priori set of FNs (to different individuals' functional connectivity) allows the investigation of (i) the functional differences among individuals under different cognitive demands [14,19,20]; (ii) aging [19,21,22]; or (iii) neurological dysfunctions [23–25]. Besides Yeo's functional FN atlas, other highly putative establishments of an a priori set of FNs were also featured in the works by Power et al. [26], Glasser et al. [27], Gordon et al. [28], and most recently in the work by Schaefer et al. [29]. The most recent review on the identification and applications of an a priori set of FN mappings can be found in the work of Bryce and colleagues [18].

In the case of human brain complex networks, higher-order interactions among neuron populations, at the whole-brain level, have been shown to unravel complementary insights that would otherwise not be fully appreciated by conventional node-based (zeroth-order) or edge-based (first-order) investigations [2,4–6,30,31]. Nonetheless, the non-local properties of topological strata induced by local/quasilocal functional sub-circuits have yet to be addressed. Specifically, higher-order characteristics induced from an a priori set of functional sub-circuits have yet to be thoroughly investigated.In brain connectomics, understanding complex behaviors arisen at a scale between the microscopic (brain regions) and macroscopic (whole-brain) levels would set the stage for a deeper, more comprehensive picture to better understand the human brain large-scale functional sub-circuitry, which, in turns, may provide foundational support to investigate individualized or task-based parcellations [32,33].

To that end, we formally explored and measured the topological invariant characteristics of an a priori set of FNs (e.g., Yeo's sub-circuitry [17]) through the first three homological dimensions: H_0 (connected components), H_1 (first-order (graph-theoretical) cycles), and H_2 (second-order cycles). These explorations on the homological properties of FNs are computed on the 100 unrelated subjects from the Human Connectome Project (HCP) dataset in which fMRI data were recorded, for each subject, in resting state and seven other fMRI tasks. The fMRI data were processed and parcellated into 360 brain regions, according to [34]. To investigate the higher-order mesoscopic properties of the constructed functional connectomes (FCs), we used the seven a priori FNs, proposed by Yeo and colleagues [17], the 14 sub-cortical regions of which were added for completeness. It is worth noting that our proposed framework can be applied to other combinations of parcellations and functional sub-circuitry partitions. Our results indicate that each homological order uniquely unravels complementary properties of human brain functional sub-circuits. Noticeably, the H_1 homological distance between rest and motor tasks was observed at both the whole-brain and sub-circuit consolidated levels, which suggested the self-similarity property of human brain functional connectivity unraveled by a homological kernel. Furthermore, at the whole-brain level, the rest–task differentiation was found to be most prominent between rest and different tasks at different homological orders: (i) Emotion task (H_0), (ii) Motor task (H_1), and (iii) Working memory task (H_2). At the functional sub-circuit level, the rest–task functional dichotomy of the default mode network was found to be mostly prominent at the first and second homological scaffolds. Also at such scale, we found that the limbic network plays a significant role in homological reconfiguration across both task and subject domains, which paves the way for subsequent investigations on the complex neuro-physiological role of such network. From a wider perspective, our framework can be applied, beyond the brain connectomics field, to study non-localized coordination patterns of localized structures stretching across complex network fibers.

The rest of this paper is organized as follows. In Section 2, we provide the formalism describing the theoretical foundation to quantify higher-order relationships of multi-scale networks. In Section 3, we present the results of applying the formalism in Section 2 to the human brain connectomics data. In Section 4, we discuss further insights of our findings. In Section 5, we conclude the paper and propose avenues for future research.

2. Formalism

The process to glean topological information for a set of data, which by itself is discrete, consists in first turning it into a graph modeling the first-order interactions and then to progress to a topological space by realizing its simplicial clique complex $\Delta(\Gamma)$, which models simultaneous, and thereby higher-order, interactions. The topological construction flow is as follows:

$$X \rightsquigarrow \Gamma \rightsquigarrow |\Delta(\Gamma)| \tag{1}$$

We stress that the first-order information yielding the graph is an additional datum, while the clique complex completes these data into a space. The topological space, which is simplicial in nature, has topological invariants associated to it, such as the homology

$H_i(\Delta(\Gamma))$ and Betti numbers b_i. The 0th Betti number b_0 counts the number of components and the first Betti number b_1 counts the number of independent loops (i.e., graph-theoretical cycles). If the graph is connected, these satisfy $b_0 - b_1 = \#$ of vertices $- \#$ of edges. The next higher interaction is b_2, which counts the number of independent spheres, or more precisely homology classes, in the realization. The realization is given by inserting a simplex for each complete graph, as seen below.

Graphs in this setting are best understood as given by symmetric matrices, the entries of which are given by the first-order interaction as witnessed by Pearson correlation functions. Defining a cut-off parameter r for the interactions then determines a graph $\Gamma(r)$ and the homology becomes a function of this r. Scanning r from 0 to 1 homology is born and annihilated. The sequence of these events is mathematically captured by persistence homology and can be encoded and visualized in terms of bar codes.

When comparing different bar codes, one usually uses the Wasserstein distance, which is a natural norm on the space of such diagram. It is not the only norm, however, and in special situations other measures are more appropriate.

2.1. Graph, Induced Subgraph, Clique Complex

In the context of this study, the graph (network) quantifying the whole-brain functional connectivity profile is called the functional connectome (FC). Induced subgraphs are utilized to model functional sub-circuits (e.g., Yeo's Functional Networks or FNs) of the FC. By construction, an FC is a complete weighted graph (See Figure 1A). The mathematical and computational setup is as follows:

Mathematically, it is a *graph/network* Γ with vertex set V and edge set of edges E where an edge in E is a two-element set $\{u, v\}$ of vertices. Enumerating the vertex set by $1, \ldots n$, a graph is equivalently encoded by its symmetric adjacency matrix $M(\Gamma)$ whose entries are $m_{uv} = 1$ if the vertices u and v are connected by an edge and 0 if not. We make the choice that the diagonal entries are 1. A graph is *complete* if there is an edge between any two distinct nodes. The matrix $M(\Gamma)$ is the matrix all of whose entries are 1. The number of edges of a complete graph is $|E| = \binom{|V|}{2} = \frac{1}{2}(|V||V-1|)$, which is the same as the number of non-diagonal independent entries in a symmetric $|V| \times |V|$ matrix. The two main topological invariants of a graph are the number of connected components b_0 and the number of loops $b_1 = |E| - |V| + b_0$, which are also called the first and second Betti numbers, of which the combination $\chi = b_0 - b_1 = |V| - |E|$ is called the Euler characteristic of the graph.

A *subgraph* is specified by a subset of nodes and a subset of edges connecting these nodes. Each graph is a subgraph of the complete graph on its vertices. This can be thought of as deleting the missing edges from a complete graph or equivalently setting the corresponding matrix entries to 0. An *induced subgraph* is simply specified by a subset of vertices. It contains all the edges connecting these vertices. If V' is the vertex subset, the matrix of the induced subgraph is given by the submatrix $M(\Gamma)_{V'V'}$. An induced subgraph is a *clique* if it is itself a complete graph; in other words, all the entries of $M(\Gamma)_{V'V'}$ are 1.

To use topological or simplicial methods such as homology, one promotes a graph Γ to a simplicial space $\Delta(\Gamma)$. This is not simply the graph itself as glued together from points and intervals, but is more involved. It is the realization of the clique complex. The construction can be understood as an iteration of gluing in simplices. An n simplex is the topological space of all vectors $(t_1, \ldots t_{n+1})$ whose entries are non–negative $t_i \geq 0$ and whose sum is $t_1 + \cdots + t_{n+1} = 1$. The dimension, which is the number of free parameters, is n. The gluing procedure starts with the 0 simplices. These are the vertices of Γ viewed as points. In the next step, one 1-simplex, which is an interval, is glued in for each edge by identifying the endpoints of the interval with the vertices the edge connects. The higher-dimensional simplices are glued in according to complete induced subgraphs. For instance, for any three vertices that are pairwise connected by edges, one glues in a two simplex, which is a triangle whose sides are the edges. At the next level, one glues in three simplices, that is tetrahedra, for each complete graph on 4 verities, which has six edges identifying the

four sides of the tetrahedron with the triangles corresponding to the three edge subsets and so on. The gluing procedure is tantamount to giving the (semi)-simplicial structure which specifies to what extent the n dimension $n-1$ boundary simplices of an n simplex are glued, in such a way that the gluing is consistent with all sub-simplices, regardless of their dimension.

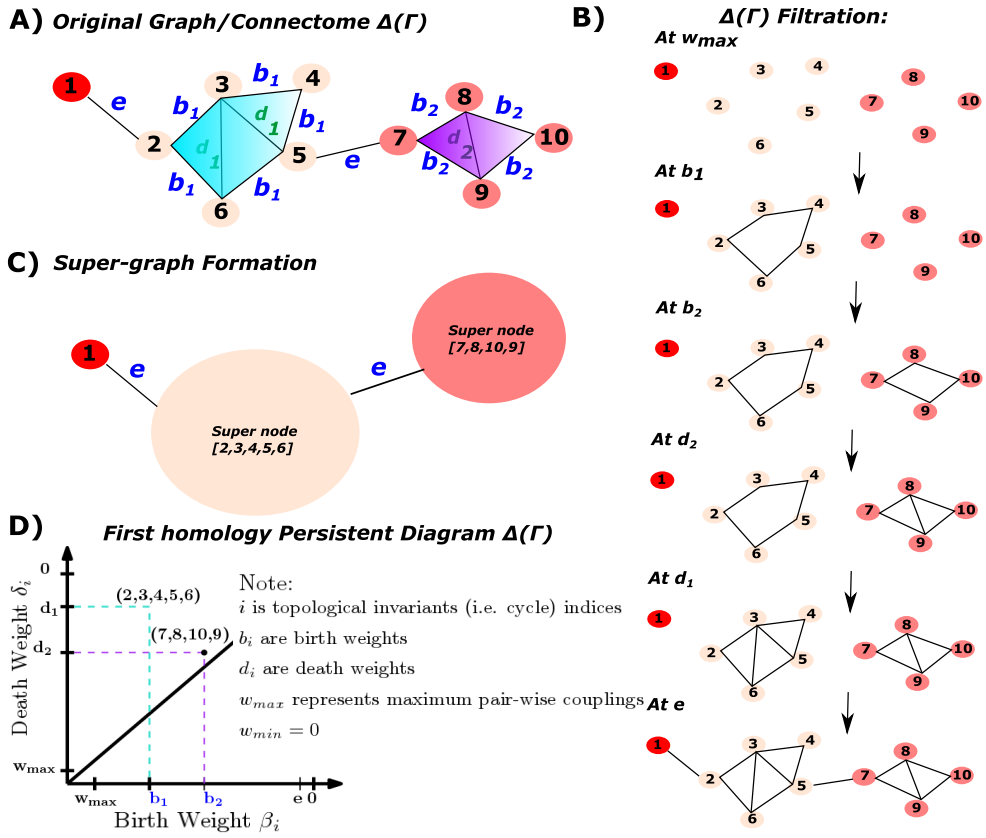

Figure 1. Topological landscape of human brain functional networks: (**Panel A**) is the schematic representation of a graph (e.g., functional connectome) modeling first-order interactions (e.g., functional couplings) with weight values $w_{uv} = d_1, d_2, e, b_2, b_1$. (**Panel B**) is a sequence of induced subgraph scaffolds (also referred to as filtration) by scanning across w_{uv} (Note that the filtration is built on $d_{uv} = 1 - w_{uv}$); hence, the starting point $\Gamma(w_{max} = 1) = \Gamma_1$ is an empty graph. (**Panel C**) represents the super-graph construction by merging all ROIs belonging to the same FN to one super-node through the equivalence relation $\bar{\Gamma} = \Gamma/\gamma$, which is defined as follows: $\gamma_1 = 1$ (e.g., FN1); $\gamma_2 = 2, 3, 4, 5, 6$ (e.g., FN2); and $\gamma_3 = 7, 8, 9, 10$ (e.g., FN3). Notice that the super graph itself is a graph; hence, homological computations that were applied in the original graph can also be applied to the super graph itself. In this example, the super-/consolidated graph has 3 super-nodes. Additionally, the weight matrix is re-scaled according to $\bar{w}_{i,j}$. (**Panel D**) is the corresponding persistent diagram for the first homology which accounts for two first-order cycles in a network: (2, 3, 4, 5, 6) and (7, 8, 10, 9); here, we see that cycle (2, 3, 4, 5, 6) lasts longer (more persistent) compared to cycle (7, 8, 10, 9). Finally, when scanning across five distinct r parameters, we obtain the zeroth and first Betti numbers: $b_0 = 10, 6, 3, 3, 3, 1$ and $b_1 = 0, 1, 2, 1, 0, 0$, respectively.

The complete graph on n vertices as space is realized to the full n simplex. Given an arbitrary graph, the realization of the clique complex has such a simplex for each complete induced subgraph and these simplices are glued together by the inclusion of subgraphs. This identifies the simplex of a subgraph of a complete graph as a side of the simplex of the graph and hence the space is glued together from maximal simplices corresponding to maximal complete subgraphs along faces corresponding to common subgraphs. One can iteratively construct this space by gluing in higher and higher simplices. This space

is higher-dimensional and has more topological invariants, the higher Betti numbers b_i of which are the dimensions or ranks of the respective homology groups H_i. The number of connected components is the same for the graph and the associated space. The first Betti number b_1 may differ depending on whether one is looking at the graph or the space. The first graph's Betti number for the complete graph is $\frac{1}{2}(|V|(|V|-3)+1$, while the first Betti number of the corresponding space, the simplex, is 0.

2.2. Filtration by Weights and Persistent Homology

Preface. A *non-negatively weighted graph* is a graph together with a weight function $w : E \to [0,1]$ on its edges. Again, after enumerating the vertices, this defines a symmetric matrix $W = W(\Gamma, w)$ with entries $w_{uv} = w(\{u,v\})$, i.e., the weight of the edge connecting u and v. If there is no such edge, the entry is 0, and the diagonal entries are fixed to be 1. Choosing a cut-off r defines the symmetric matrix $W(r)$ whose entry $w(r)_{uv} = 1$ if $w_{uv} \geq r$ and 0 if $w_{uv} < r$. It has 1's on the diagonal and defines the graph $\Gamma(r)$. Note that $\Gamma(0)$ is the original graph and $\Gamma(1)$ is the graph on the vertex set with no edges. Let $\bar{W}$ be the order set containing unique weight values, in decreasing order, in matrix W, varying the threshold parameter r from 0 to 1, which defines a sequence of subgraphs as follows (See Figure 1B):

$$\Gamma(1) \subset \Gamma_1 = \Gamma(r_1) \subset \Gamma_2 = \Gamma(r_2) \subset \cdots \subset \Gamma_{\bar{W}} = \Gamma(r_{|\bar{W}|}) \subset \Gamma = \Gamma(0). \tag{2}$$

with $1 > r_1 \cdots > r_{|\bar{W}|} > 0$ and the Γ_j are the finitely many different graphs that appear. At each stage j, some edges are added from the lower stage $j-1$. The graph $\Gamma(1)$ is the subgraph with the full vertex set, whose edges are given by the non-diagonal entries 1. In practice, if the weights are Pearson correlations functions, the only entries of 1 will be along the diagonal and the graph $\Gamma(1)$ is simply the discrete set of data.

Note that, since set W describes diatic functional couplings (e.g., similarity) between two nodes of a network (or brain regions of interest (ROIs) in this formalism), this implies that the "distance" (e.g., dissimilarity) between two nodes is defined as follows:

$$d_{uv} = 1 - w_{uv} \tag{3}$$

In other words, with this setup, we ensure that

- Γ_1 is essential the 1-skeleton scaffold where all nodes are perfectly coupled ($d_{uv} = 0$), which results in an empty graph.
- Γ_{j_1} is always an induced subgraph of Γ_{j_2} for all $j_1 < j_2 \leq |\bar{W}|$.
- The sequence $\{\Gamma_l \mid l \in [\bar{W}]\}$ starts with an empty graph (homeomorphic to $\mathbb{Z}_n$) and ends with a complete graph (or a clique of n nodes) (homeomorphic to simplicial complex of size n, i.e., K_n).

Given a filtered system, that is, a sequence of inclusions of spaces as (2), one can utilize the tool of persistence homology to track the changes in the fundamental topological invariants of homology and Betti numbers. This supplies a characteristic for the whole sequence. We wish to stress that it is the sequence that is of importance here. The two endpoints have rather trivial topological properties. If the start is just the data, then this is a discrete set, and at the other end the space is just a full simplex corresponding to the complete graph, which is contractible. The transition from one to the other and the appearance—and disappearance—of higher homology is what is kept track of by persistent homology.

Bar codes and distances between them. The fingerprint is the variation which is quantified by the bar codes. The variation parameter is the parameter r introduced above. A bar code is a type of signature for the variation. For each persistent homology class, it records the value of the parameter r_{ini} when a representative appears (birth) and the value r_{fin} when it disappears (death) (See Figure 1D). This is an interval (or bar) $[b(c) = r_{int}, d_(c) = r_{fin}]$. At any given r, the homology is given by those classes c for which $r \in [b(c), d(c)]$. In the variation, all higher-homology classes are born and eventually die. The 0-th homology starts with as many classes as data points and then eventually

decreases (classes die) until there is only one class left, which implies that the space is connected. The bar code is equivalently encoded by the persistence diagram which the set with multiplicity (multiset) of all the endpoints of the bars $\{(b(c), d(c))\}$. This is in fact a multi-set, since some of the classes may appear and die at the same parameter values and these multiplicities are recorded, e.g., $(0.2, 0.8)$ with multiplicity 2, which means that there are two bars of this type. Its pth part, Dgm_p, is given by a bar corresponding to classes of homological dimension p.

Topological distance formulation. The Wasserstein distance is the natural norm on the diagram space, e.g., the birth–death diagram of topological features. The Wasserstein distance is the right measure for processes, taking one diagram to another in a varying family—now of persistence diagrams. This is well suited for analyzing a basic underlying setup with variations. This is commonly viewed and addressed as the stability theorem. In our case, we use Wasserstein distance to compute the distance between two diagrams for the first and second-order homology (e.g., $p = 1, 2$) in various scenarios (e.g., comparing topological behaviors between the same functional networks at resting conditions).

Specifically, for a fixed homological order p (in this paper, $p = 1, 2$), the $q-$Wasserstein distance $D_{W,q}$ ($\forall q > 1$) for two persistent diagrams $Dgm_p(X)$ and $Dgm_p(Y)$ for two datasets X, Y can be defined as follows [35]. For a single interval $I = [x, y]$, set $d(I) = \frac{1}{2}(y - x)$, which is the distance to the diagonal of the point (x, y) in $\mathbb{R}^2$. For two intervals $I = [x_1, y_1], J = [x_2, y_2]$, define their distance as $d(I, J) = \max(|x_2 - x_1|, |y_2 - y_1|)$. This is the max norm distance for the two points $(x_1, y_1), (x_2, y_2)$ in $\mathbb{R}^2$. A partial pairing between two sets S and T is a choice of subsets $S_0 \subset S, T_0 \subset T$ and a 1-1 correspondence between the two subsets $\pi : S_0 \Longleftrightarrow T_0$. This extends to sets with multiplicity by choosing multiplicities of elements and matching them with multiplicity. Given diagrams $Dgm_p(X), Dgm_p(Y)$, let Π be the set of all partial pairings then. The Wasserstein distance minimizes the sum of three contributions: the distances between intervals that are paired and two contributions of the distance to the diagonal for intervals that are not paired. It minimizes over two possible scenarios, namely points moving and points moving in and out of the diagonal. The first means that the classes shift in their rates and the second means that the classes vanish from the diagram and new classes are introduced. Given π, let $Dgm_p(X)_1 = Dgm_p(X) \setminus Dgm_p(X)_0$ and $Dgm_p(Y)_= Dgm_p(Y) \setminus Dgm_p(Y)_0)^q$ be the complements.

$$D_{W,q}(Dgm_p(X), Dgm_p(Y))) = \min_{\pi \in \Pi}[\sum_{I \in Dgm_p(X)_0} d(I, \pi(I))^q + \sum_{I \in Dgm_p(X)_1} d(I)^q + \sum_{J \in Dgm_p(Y)_1} d(J)^q]^{\frac{1}{q}} \tag{4}$$

In the zeroth-order homology, the Wasserstein distance becomes an unnatural choice. This is due to the fact that the data points are the 0–classes and they are all born at $r = 0$. Thus, a contribution as disappearing or appearing from the diagonal which signifies being born at different times is not a possible scenario.

It is better to consider $Dgm_0(X)$ just as the multiset of endpoints of the bars $[0, d(x)]$ where $x \in X$ and use the classical Hausdorff distance to measure the (dis-)similarity between two point clouds living in $\mathbb{R}$. This specialized to:

$$D_H(Dgm_0(X), Dgm_0(Y)) = max \max_{x \in X} \min_{y \in Y} |d(x) - d(y)|, \max_{y \in Y} \min_{x \in X} |d(x) - d(y)| \tag{5}$$

2.3. Functional Connectomes and Mesoscopic Structures

Mesoscopic structures are typically referred to as structures whose elements are proper subsets of a system's elements. In the brain connectomics domain, there are two types of mesoscopic structures: localized/quasilocalized and non-localized (topological strata). In this section, we provide an overview and definition of each type in the context of brain connectivity.

2.3.1. Localized Mesoscopic Structures

Localized mesoscopic structures are sub-systems that are learned from local network properties such as nodes or edges, or correlations among neighboring nodes. In brain connectomics, these sub-structures are induced from a wide array of techniques, including but not limited to clustering [17,26] or low-dimensional approximation of high-dimensional dynamics [36–39,39]. The most commonly known localized mesoscopic structures in brain networks are often referred to as functional sub-circuits or functional networks [10].

Definition 1 (Definition adapted from [40])**.** *An a priori set of functional networks (FNs) represents sub-circuits (or equivalently, sub-networks) that are highly reproducible across individuals at resting condition (absence of task-induced cognitive demand). Hence, FNs are also known as resting-state networks (RSNs).*

Special collections of induced subgraphs are used to group brain regions of interest (ROIs) into localized/quasilocalized mesoscopic structures of brain functions denoted as functional sub-circuits or, equivalently, functional networks (FNs). A collection of k subgraphs (of graph Γ) is denoted as $\{\gamma_i \subset \Gamma \mid i \in [k]\}$. A collection of induced subgraphs is *a vertex covering* if in the graphs each vertex of Γ is a vertex of one of the γ_i.Such a vertex covering is disjoint if the γ_i have disjoint vertices. After enumerating all nodes by $1, \ldots, n = |V|$, the collection of induced subgraphs is fixed by the membership assignment. This is specified by a partition vector denoted as $\sigma \in [k]^n$, where $\sigma = [\sigma_u] = i \in [k]$, indicating that u belongs to $\gamma_i \mid i = \{1, 2, ..., k\}$. Note that, in network science, FNs are equivalent to the term "communities" [11–13,41]. The problem of identifying the set of communities $\{\gamma_i \subset \Gamma \mid i \in [k]\}$ for a given complex network is called the community detection problem [11–13,41].

2.3.2. Non-Localized Mesoscopic Structures

While studies of network properties and dynamics using locally featured properties (nodes, edge attributes) provided a well-grounded approach, these methods were proven to be cumbersome in describing and quantifying heterogeneity existing across network dynamical fabrics. These structures usually encompass many body interactions or encapsulate topological sub-structures that cannot be mathematically described using local attributes. To that end, homology [42] offers a unique capability to capture the so-called non-localized mesoscopic structures which, otherwise, cannot be reduced to local or quasilocal network properties. In the context of weighted complex networks, persistent homology is used to identify how long (the persistence of) a hole (at any given dimension) lasts from its birth (the weight scale $w_B^* \in [0, 1]$ at which the hole is observed) to its death (the weight scale $w_D^* \in [0, 1]$ at which the hole is filled).

In the context of functional brain connectivity, non-localized mesoscopic structures in an FC represent the encapsulated area wherein there is *less* functional connectivity collectively formed among brain regions encapsulating these structures [43]. Such structure characterizes the notion of hole; the boundary that wraps around these structures are the non-localized mesoscopic fabrics characterized by the so-called cycles. These cycles exist in different homological dimensions for a given networked system, which can be described in the language of a manifold. The hollow structures (holes) could be seen as overarching wraps around special hollow structures in a manifold with different characteristics and properties, compared to functional networks [17,44–46] or communities [11,12,41,47] in complex networks.

2.4. Consolidated/Super Graph

The system under consideration is naturally regarded as a two-level system given by the ROIs and their connections. The first level is made up of the individual ROIs and the second level is given by the connections between the ROIs. In graph theoretical language, the full graph $\Gamma(r)$ containing all the nodes naturally has a subgraph $\gamma_i(r) \subset \Gamma(r)$.

These subgraphs form a supergraph, which has the subgraphs as new vertices and has the edges between two vertices if there are edges between the subgraphs (See Figure 1C). There are two versions, the first is the multi-edged graph that is described theoretically by contracting all the edges of the subgraphs γ_i, that is, if $\gamma = \cup_i \gamma_i$ is the union of subgraphs, then $\bar{\Gamma} = \Gamma/\gamma$. Reducing possible multiple edges to just one edge on has the reduced graph $\bar{\Gamma}^{red}$, which is again an ordinary graph described by a matrix. For a weighted graph, assuming that the subgraphs are not connected, the graphs γ_i correspond to block matrices along the diagonal and the edges of the quotient graph are the off-block entries. To obtain a matrix, one can consolidate the weights into one weight by choosing a function $W_{i,j} = f(w_{u_k,v_l}), w_{u_1,v_2}, \ldots, w_{u_1,v_k}, w_{u_2,v_1} \ldots, w_{u_l,v_k}$ where $u_1, \ldots u_l$ are the vertices of γ_i and $v_1, \ldots, v_l$ are the vertices of γ_j. One such choice is $W_{i,j} = \sum_{u \in \gamma_i, v \in \gamma_j} w_{u,v}$ and then it is normalized to

$$\bar{w}_{i,j} = W_{i,j}/max(W_{i,j}) \tag{6}$$

In the case under consideration, the graph $\bar{\Gamma}$ has eight (super-)vertices corresponding to each FN. The basic topological invariant of the loop number is of great interest as it is a measure of the inter-connectivity of these "super-regions". The persistent homology for the normalized super graph, that is, the consolidated graph, will then complement this information to show clusters of correlations between FNs.

3. Results

3.1. Data

Human Connectome Project (HCP) Dataset. We used the master data release extracted from the HCP Young Adult (HCP-YA) subject release [48]. Specifically, the fMRI dataset was obtained from the HCP repository (https://www.humanconnectome.org/, accessed on 1 September 2021), with Released Q3. The full release of the Q3 HCP dataset has 889 subjects with complete data for all four 3T MRI modalities following the HCP protocol. While many of them are from the same family, we only collected 100 genetically independent subjects for this study. In general, all MRI neuroimaging modalities were acquired in two different days, with two different scanning patterns (e.g., phase acquisitions: left-to-right or LR and right-to-left or RL). The detailed description is in the next section and Figure 2.

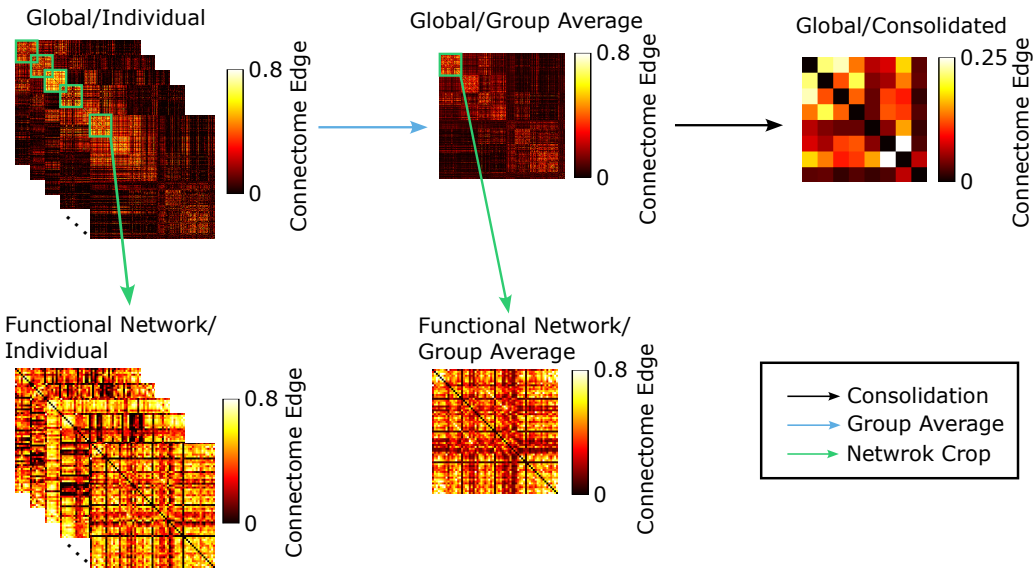

Figure 2. fMRI whole-brain connectome multi-level analysis workflow. For each task, we started with individual-level functional connectome. On the global (macroscopic) level, we conduct individual analysis as well as group-averaged analysis, and the functional network (mesoscopic) level extracts functional networks from either the individual or group-averaged macroscopic graph. The consolidated graph is constructed by aggregating the nodes from the group-averaged macroscopic level connectome. The scales in each panel represent the strength scale of functional connectivity.

HCP Functional Data. The fMRI data from the 100 unrelated subjects in the HCP Q3 release were employed in this study [48,49]. Following the HCP protocol, all subjects had provided written consent to the HCP consortium. The two resting-state functional MRI acquisitions with HCP filenames: $rfMRI_REST_1$ and $rfMRI_REST_2$ were collected in two separate sessions (on two different days), with two distinct scanning acquisitions (LR and RL) for each day, see [34,48,49] for further details. Besides the resting state, the dataset also includes fMRI data from seven (07) fMRI tasks: gambling ($tfMRI_GAMBLING$), relational or reasoning ($tfMRI_RELATIONAL$), social ($tfMRI_SOCIAL$), working memory ($tfMRI_WM$), motor ($tfMRI_MOTOR$), language ($tfMRI_LANGUAGE$), and emotion ($tfMRI_EMOTION$). Per [34,50], three following fMRI tasks were obtained on the first day: working memory, motor, and gambling; the rest were obtained on the second day. The local Institutional Review Board at Washington University in St. Louis (scan site) approves all the scanning protocols used during the HCP dataset acquisition process used in this paper. Please refer to [34,50,51] for a further detailed description of the HCP-YA dataset. The data were pre-processed following the HCP functional pre-processing guidelines [34,51]. In summary, the processing steps included the removal of artifacts, motion correction, and registration to the standard Montreal Neurological Institute space. Additionally, weak high-pass temporal filtering (at least 2000s full width at half maximum) was applied to both formats to remove slow drift. Furthermore, artifacts and motion-related time courses (including the six rigid-body parameter time series, their backward-looking temporal derivatives, plus all 12 resulting regressors squared) were regressed out from both volumetric and grayordinate data [51]. Note that all tasks and resting functional MRIs were treated with equal importance. In this work, we denote seven fMRI tasks as gambling (GAM), relational (REL), social (SOC), working memory (WM), language processing (LANG), emotion (EMOT), and motor (MOT). The abbreviations for these tasks are used in the tables and figures for the following macroscopic, consolidated, as well as mesoscopic analyses.

Table 1 depicts basic information about the fMRI conditions' run time and the number of time points for each task. Subsequently, along with Table 1, a brief description of each fMRI condition is provided below. An extended description is provided in the HCP manual (https://www.humanconnectome.org/storage/app/media/documentation/s1200/HCP_S1200_Release_Reference_Manual.pdf, accessed on 1 September 2021).

1. REST: Eye open with relaxed fixation on a bright cross-hair with dark background. A total of 1200 time points were obtained with 720 ms TR.
2. EMOTION: Subject was instructed to match two faces (or shapes) shown from the bottom to the top of the screen. Faces were shown with angry/fearful expressions. Each scan involved three face blocks and three shape blocks with eight seconds of fixation.
3. GAMBLING: Implied a card-playing game wherein the subject needed to guess a number of cards in order to win or lose money. At each trial, the subject was instructed to guess whether a card had a value greater or smaller than 5, given that the numerical range of the cards was between 1 and 9. The subjects had 1.5 s to respond and 1 s of feedback.
4. LANGUAGE: At each scan, four blocks of story tasks and four blocks of math tasks were presented to the subject. The stories contained brief auditory information followed by a choice of questions about the story topics. The math tasks contained arithmetic questions with a similar level of difficulty compared to the story task.
5. MOTOR: The subjects were shown various cues and instructed to either tap (left and right) fingers, squeeze (left or right) toes, or move their tongue in response to different areas of the human brain motor cortex. The task contained a total of 10 movements (12 s per movement), preceded by a 3-s cue.
6. RELATIONAL: The subjects were presented with six shapes along with six different textures. Given two pairs of objects (one on the top and the other one at the bottom of the screen), the subject had to decide whether the shape (or texture) differed across

the pair on the top screen. In addition, they had to decide whether the same difference was carried over to the bottom pair.

7. SOCIAL: The subjects were shown a 20-s video clip containing randomly moving objects of various geometrical shapes (squares, circles, triangles, etc.). After that, the subjects were instructed to respond to whether these objects had any mental interactions (shapes took into account feelings and thoughts), and respond by either Undecided or No Interactions.
8. WORKING MEMORY: The subjects were presented with trials of tools, faces, and body parts. Four different stimulus types were presented in each run. In addition, at each run, two types of memory tasks were presented: two-back and zero-back memory tasks.

Table 1. fMRI task scanning length and number of frames description. All fMRI task run times were reported in order of minutes and seconds. Except for the resting state (for which each subject was scanned twice per day for a total of $2 \times 2 = 4$ sessions), all other tasks had two scans (RL and LR). TR is the time between two consecutive readings.

fMRI Conditions	Run Time (min:s)	# of Time Points
REST1 (and REST2)	14:33	1200
EMOTION (EMOT)	2:16	176
GAMBLING (GAM)	3:12	253
MOTOR (MOT)	3:34	284
LANGUAGE (LANG)	3:57	316
RELATIONAL (REL)	2:56	232
SOCIAL (SOC)	3:27	274
WORKING MEMORY (WM)	5:01	405

Brain atlas. The brain atlas used in this work is based on the cortical parcellation of 360 brain regions proposed by Glasser and colleagues [27]. Similarly to the description in [14,52,53], 14 sub-cortical regions were added for completeness, as provided by the HCP release (filename *Atlas_ROI2.nii.gz*). We accomplish this by converting this file from the NIFTI to the CIFTI format, using the HCP workbench software (https://www.humanconnectome.org/software/connectome-workbench, version 1.5.0, accessed on 1 September 2021) through the command -cifti- create-label. We then obtained a brain atlas of 374 brain regions (360 cortical + 14 sub-cortical nodes) registered to a common space which allowed us to parcellate fMRI voxel-level BOLD time series into the brain region of interest for the level time series (command: -cifti-parcellate). Time series were z-scored by using the command -cifti-math.

Estimation of functional connectomes. Parcellated time series were then used to construct the whole-brain functional connectivity by computing the Pearson's correlation coefficients for each pair of brain regions. This operation can be completed using the *Matlab* command -corr, which results in a symmetric matrix. All entries in the whole-brain FCs were applied the absolute values so that the threshold parameter was $r = [0, 1]$.

The mapping of functional networks onto FCs. After each subject was registered to the appropriate common space and properly parcellated according to Glasser's parcellation, we explored the topological features of human brain functional connectivity (FC) by further subdividing whole-brain FC into resting-state networks (equivalently referred to as functional networks/communities), as seen in [17]. Yeo's seven functional networks create a many-to-one mapping that clusters a subset of brain regions into a single region of interest, which in total results in seven ROIs in the brain cortical region. The parcellation was developed by clustering the functional coupling for each subject separately [54] and finds the maximum agreement on the cluster label membership. This particular partition includes seven functional networks (FNs): Visual (VIS), SomatoMotor (SM), Dorsal Attention (DA), Ventral Attention (VA), Limbic (LIM), Frontoparietal (FP), Default Mode Network (DMN); and Sub-cortical (SUBC) region which is, as mentioned above, added into this atlas for

completeness. Consequently, the parcellation comprised eight (8) FNs for each subject/task (the abbreviation of those functional networks will be used in the following figures with the mesoscopic analysis).

3.2. Group Analysis: Macroscopic WHOLE-BRAIN LEVEL

Topological differences between rest and fMRI tasks. We first explored the topological distances at the group-average whole-brain connectivity level between resting state and fMRI task activation states (see Figure 3 and see Figure S1 for the persistent diagram at the macroscopic level). Each homological group consists of three figures; the first one is the bottom left heatmap, representing the pair-wise Wasserstein distance. The bottom right bar plots show the average distance between one task to all other tasks; thus, the task with the highest average distance will indicate its high differentiation to other tasks. Finally, the top right plot shows the variance of each task looking at their distance from the other tasks. Specifically, the zeroth homology suggests that the relational task is the most different from the emotion task. Indeed, other studies, such as [14] through the network morphospace mechanism, have also suggested that relational and emotion tasks activate minimally-to-none overlapping functional circuits of the human brain. In terms of H_0 (i.e., connected components), the relational task is also the most distinctive task, compared with others (highest average); the relational task is followed by the resting state on the average difference with other tasks.

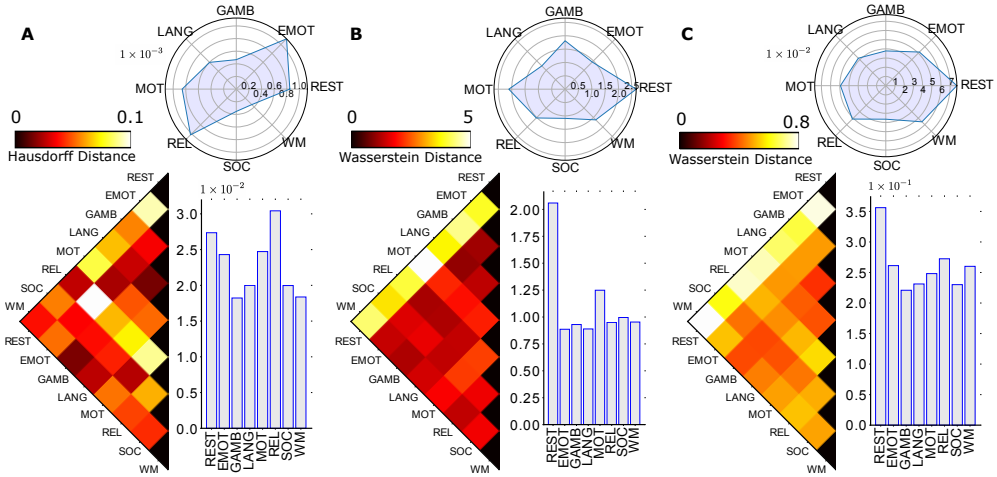

Figure 3. Group-average macroscopic homological distances between fMRI tasks and rest. Specifically, three panels (e.g., left, middle, and right) represent the zeroth (**Panel A**), first (**Panel B**), and second (**Panel C**) homological distance, respectively, between fMRI tasks and resting condition. Group-average FCs are computed by taking the average of all subjects in the 100 unrelated subjects dataset sampled from the HCP project. The zeroth homological distance is computed using the Hausdorff formula (measured between persistent diagrams of two FNs extracted from group average FC), while the first and second homology distances are computed using the Wasserstein formula. Each panel in the graph is composed of three different components, the left triangular heatmap represents the distance, with its color bar indicating the scale above the heatmap; the bar plots represent the average distance to other tasks; and the circular plots represent the variance among all fMRI tasks. Complete names of each task include resting (REST), emotion (EMOT), gambling (GAM), language processing (LANG), motor (MOT), relational (REL), social (SOC), and working memory (WM).

Moreover (see Figure 3B), the first homology exhibits the highest degree of differentiation between the resting state and the task-positive state, as measured by the average of the first homological Wasserstein distance between rest and task bar codes. The first homology also suggests that the motor task is the most topologically different task, compared to the resting state. This finding was consistent with the current literature (e.g., Amico and colleagues [16]) which stated that the motor task exhibited the most distant "within-functional

network" edges, relative to other fMRI tasks in the HCP dataset. This result also suggests that, at a global scale, the motor cortex, whose brain regions are largely employed by the motor task, modulates increasing functional activities through forming global transduction pathways with "loop-like" feedbacks (e.g., first-order cycles).

3.3. Group Analysis: Consolidated Graph $\bar{\Gamma} = \Gamma/\gamma$

With the construction of consolidated graphs, we generated a smaller-scale representation of the brain connectome to eight super nodes, which includes seven Yeo functional networks and one node for subcortical regions. Here, the super graph is constructed using the equivalence relation at the node level. As such, $\bar{\Gamma} = \Gamma/\gamma$ such that $\gamma = u \sim v \mid \sigma_u = \sigma_v, \forall u, v \in V$. In other words, all brain ROIs which belong to the same functional network are contractible.

Since the graph is much smaller, no birth was detected for a 2D simplicial complex in the filtration process; thus, only zeroth and first homology were included in the analysis (see Figure 4 and see Figure S2 for the persistent diagram at the consolidated level). In the consolidated setting, we found that the social–resting task pair had the highest distance with the zeroth homology, indicating that, at the Yeo functional network level, the connectivity representation captured more differences in the social task and resting states (see Figure 4A). By the nature of zeroth homology, where we are looking at connected components, the different most-distinct task pair between the global level and consolidated level indicates that the choice of representation could impact the topological configuration in brain connectivity. However, the Wasserstein distance between different tasks in the first homology-revealed topological invariant among both the global scale as well as the node-aggregation scale, as the resting state and motor task pair also have the highest distance measure (see Figure 4B).This consistency validated the robustness of the first persistent homology class in disentangling the brain's functional circuits. In addition to the consistency in the most distinct task pair, the resting state task also consistently appears as the most differentiated task compared to other tasks based on the average distance for each task [55,56]. This indicates that there is a significant reorganization in brain connectivity when people engage in activities from a resting state. Especially for motor tasks, it engages more different brain regions than other tasks, and thus it is also the second distinct task as it is the task that requires responses involving movement.

3.4. Group Analysis: Functional Network (Mesoscopic) Level

In previous sections, we calculated the Wasserstein distance between different tasks, where all of the nodes in the brain connectome were included. In order to assess for a given task, how the brain connectivity shifts from one functional network to another, we also conducted mesoscopic level analysis by extracting the eight functional networks from the group-averaged global graph. Since previous discoveries showed that the resting state task involves brain regions that are most distinct from other tasks, and the Yeo functional network was also optimized on the resting-state fMRI, we focused our analysis on the distance between functional networks in the resting-state task and the mesoscopic level's topological configuration (see Figures S3–S9 for the analysis of the remaining seven tasks).

3.4.1. Resting State Analysis

Fixing the task and extracting functional networks enabled the characterization of within-brain connectivity and the identification of unique topological patterns in functional networks. Particularly, the default mode is present in the pair with the largest Wasserstein distance in H_0, H_1, and H_2 homology, and it also has the largest average Wasserstein distance in H_1 and H_2 analysis (see Figure 5), suggesting a significant level of functional specialization within the default mode during the resting state. Extensive studies in the literature have validated that the default mode is more active and involved in introspective processes and is typically deactivated in the engagement of goal-oriented tasks, which is referred to as the "resting state dichotomy" of default mode network [57–59]. This finding

further reassured the robustness of the capability of the topological system to detect unique features in certain activities.

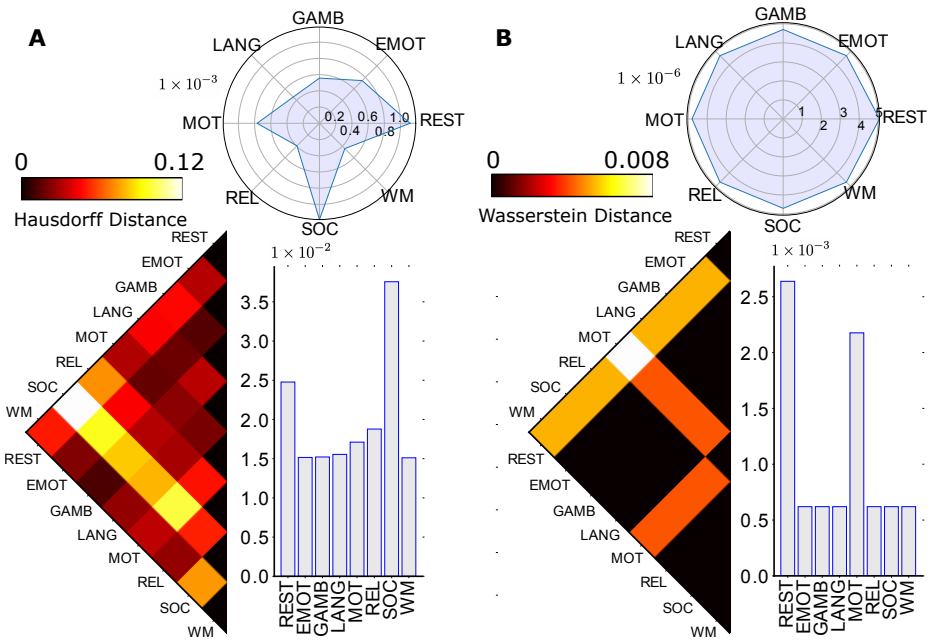

Figure 4. Consolidated homological distances between fMRI tasks and rest. The left and right panel represents the distance between tasks in zeroth (**Panel A**) and first (**Panel B**) homology, calculated by Hausdorff distance and Wasserstein distance, respectively. Each panel also contains three components, including the task-wise distance, the average distance, and the variance plot. Due to the small size of the consolidated graph, there was no second homology detected in the corresponding topological space.

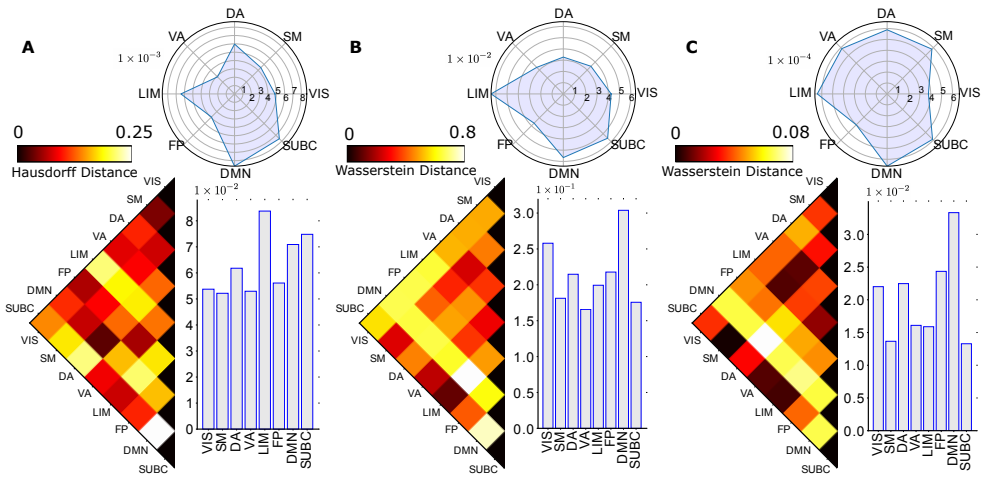

Figure 5. Group-averaged homological distances between brain circuits (FNs) at rest (e.g., resting-state networks). Three panels are positioned similarly to previous figures where they represent the distance of zeroth homology (**Panel A**), first homology (**Panel B**), and second homology (**Panel C**) between pairs of FNs. Group-averaged FNs are extracted based on Yeo's parcellation. The zeroth homological distance is computed using the Hausdorff formula while the first and second homology distance are computed using the Wasserstein formula. Each panel contains the triangular distance heatmap, the average distance bar plot, and the variance circular plots among functional networks. Complete names for functional sub-circuit include Visual (VIS), SomatoMotor (SM), Dorsal Attention (DA), Ventral Attention (VA), Limbic (LIM), Frontoparietal (FP), Default Mode Network (DMN), and Sub-cortical (SUBC).

In addition, we also discovered that the limbic system has the highest average Wasserstein distance in the zeroth homology, indicating that it is the most distinct functional network when we compare the pattern of connected components between functional networks [16,60] (see Figure 5A). The limbic system is known for its role in memory- and emotion-related activities [61–63], and the distinct connectivity pattern discovered reveals that there may still be some memory or emotional processing even during the resting state. Furthermore, the results can also serve as an indication of the individual heterogeneity in their resting-state behavior, which may involve slight mind activities. The high level of differentiation in the H_0 task pair with the limbic system is also reconfirmed in the mesoscopic level analysis in the emotion task and working memory task (see Figures S3A and S9A).

3.5. Individual Subject Analysis

While the group-averaged level connectomes (global level, consolidated level, and mesoscopic level) provide topological insights into a collective pattern, transitioning to the individual level could further offer a more personalized perspective with after-persistent-homology group insights. Moving beyond the aggregation of group data, individual-level analysis would also allow the consideration of inter-individual variability and consistency across different scales to bring even more robustness to the experimental design. Similar to the previous setting, we investigated the individual global level with consensus voting as well as the individual mesoscopic level with Kullback–Leibler divergence (KL divergence), respectively [64].

3.5.1. Macroscopic Whole-Brain Level

With 100 unrelated subjects from the HCP database, the individual macroscopic level analysis contains 100 independent persistent homology results with pair-wise task distances.At the individual macroscopic analysis, we still used the Hausdorff distance for the zeroth homology and the Wasserstein distance for the first and second homology. We evaluated the most distinct pair of tasks in each individual and Figure 6 shows the number of times each pair of tasks appeared as the most differentiated task pair.

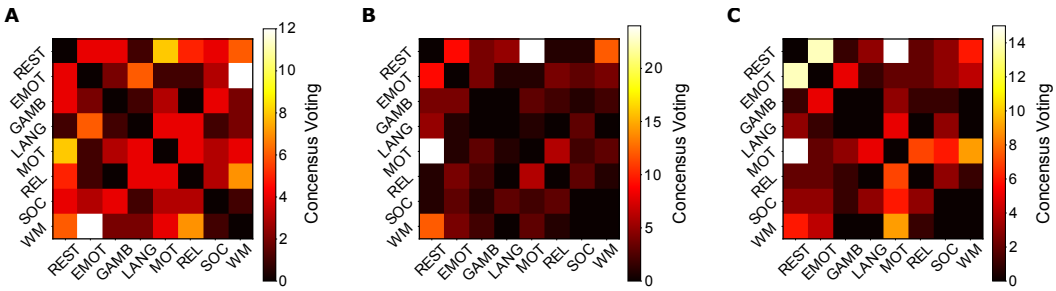

Figure 6. Individual consensus heatmap between tasks at the macroscopic level. Distance matrices between functional networks in 100 unrelated subjects were collected, and for each pair of functional networks, the frequency of it appearing as the most distinct pair among 100 subjects was counted, resulting in a majority voting heatmap for 3 homology groups ((**Panel A**) is the zeroth homology, (**Panel B**) is the second homology, and (**Panel C**) is the third homology). The number in the voting matrix represents the number of times the corresponding pair revealed the highest distance in one subject, and all numbers in one heatmap triangle should sum up to 100 for 100 subjects.

Particularly, the zeroth homology displayed the largest variability with the max count of the task pair being the smallest among the three homology groups, thus resulting in a more diffused pattern in the consensus-voting heatmap (see Figure 6A). This serves as another explanation for the impact of the choice of graph representation on the zeroth homology analysis that is relatively more varied. However, we also see the resting–motor task pair as one of the task pairs that have a high frequency at the individual level H_0 results. Furthermore, the first homology still demonstrates the consistency with the group-averaged macroscopic level as well as consolidated level analysis, where it not only has

the motor task–resting state as the most frequent task pair, but the max count is also the highest, indicating the robustness of the first homology in identifying a brain connectivity pattern with different activities (see Figure 6B). The second homology also shows the motor task–resting state pair as the most frequent task pair, which further validates our findings shown above (see Figure 6C). The individual level analysis on the macroscopic level adds another layer to the group-averaged level analysis, where either the variability in the zeroth homology or the consistency in the first and second homology both further agree with the interpretation from previous sections.

3.5.2. All-to-REST, Mesoscopic Analysis

At the individual mesoscopic level, the amount of analysis increased dramatically, with 100 individuals, eight tasks, eight functional networks, and three homological classes. In this case, it is difficult to analyze the distance between homology groups as we did at the group-averaged level. As validated in previous studies as well as our macroscopic level analysis, the resting state analysis tends to be the most distinct task compared to other tasks that include some activity engagement [16]. Therefore, we collected individual level all-to-REST distances and compared them across the functional network dimension and task dimension.

For the mesoscopic level in an all-to-REST setting, we picked three functional network pairs that have the highest distance measure from the group-averaged results (Section 3.4.1) for all three homology groups. For each pair of functional networks, we collected 14 vectors, with each FN having seven vectors containing 100 individual level distance measures between the seven non-resting-state tasks and resting-state tasks (see Figure S10), and then we compared the KL divergence between the two functional networks with vectors from the same non-resting-state task (Figure 7). In other words, the KL divergence measures the difference between two distributions (two functional networks, respectively, for all subjects) of the distance measure between the non-resting-state task and the resting-state task.

For zeroth homology, we find that the social task is more differentiated from the resting state compared to others when we consider functional network pairs of dorsal attention and subcortical, as well as the visual network with the limbic system (see Figure 7, panel B,C). These results take into consideration both task activities and interactions between functional networks at the same time, indicating that the selected pair of functional networks has very different brain connectivity configurations in social tasks compared to the resting state. The default mode is still involved in the most selected pair of functional networks in the resting state, and the relational task has a very high KL divergence compared to the resting state in many functional pairs for the first and second homology, including default mode with limbic, subcortical, visual, dorsal, and ventral attention (see Figure 7, panel D–I).

3.5.3. All-to-REST, Task Analysis

The task analysis in an all-to-REST setting provided another perspective from which the observation of functional network reconfiguration from resting state to other tasks is highlighted. In this case, we fixed the task that compared with the resting state and focused on the KL divergence between all pairs of functional networks in the first phonological order (see Figure 8 and see Figures S11 and S12 for the zeroth and second homology). To demonstrate the reconfiguration from resting to other tasks, we selected the top five largest KL divergences for each task and ranked them by the line strength in the circular plot.

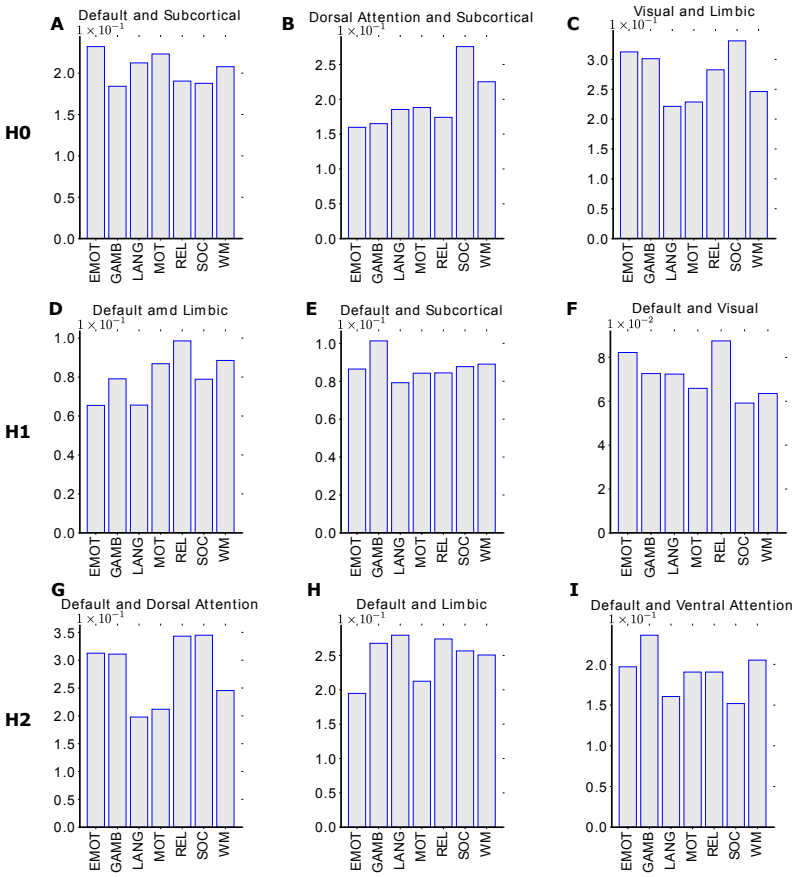

Figure 7. KL divergence plot for the top three functional network pairs in all-to-RESTING setting. Rows represent homological groups ((**Panels A–C**) are the zeroth homology, (**Panels D–F**) are the first homology, and (**Panels G–I**) are the second homology) and each has three panels consisting of the top three most distinct pairs of functional networks inferred from the group-averaged mesoscopic analysis. The bar plot demonstrates the KL divergence between the selected pair of functional networks, in terms of the 100 individual-level distance between the resting state with other tasks.

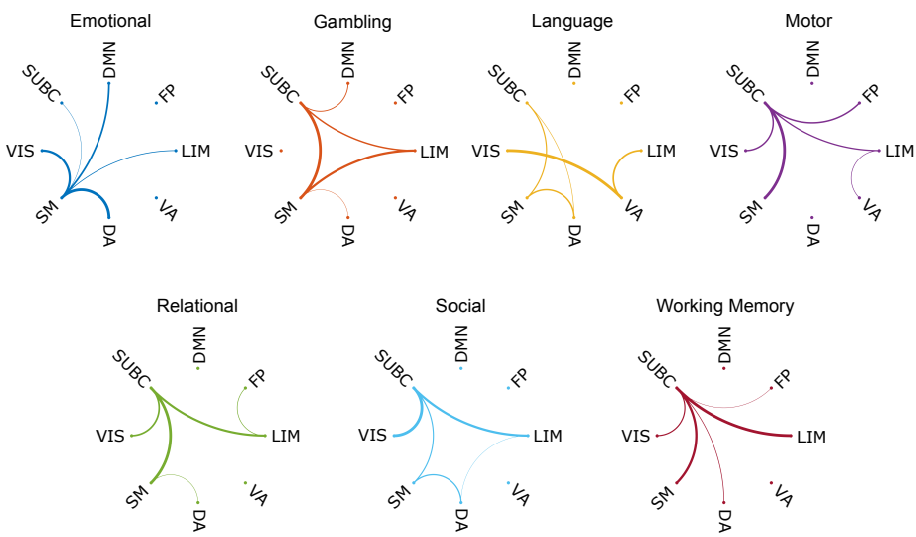

Figure 8. KL divergence circular plot for 7 fMRI tasks-to-RESTING with functional network comparison in H_1. Here, we fixed the task which compared with the resting state and visualized the top five KL divergences between functional networks. The KL divergence is normalized with regard to the top five measures and demonstrated by the strength of circular connectivity.

Some of the tasks displayed very unified patterns, such as the emotion task and the working memory task, where all the highest KL divergences included one functional network (see Figure 8, emotion, and working memory panel). The observation drawn from those two tasks showed that the reconfiguration from resting state to emotion task actually involves a significant amount of activities for somatomotor, and shifts to the working memory task will require the subcortical region to take the most response. The somatomotor network includes most of the somatosensory area, which is closely related to emotional regulation, and the subcortical region is known to be involved in complex activities such as memory-related activities. In addition, we also observed that the somatomotor network also has the strongest link in the motor task, and the subcortical region is present as the dense connectivity hub in many task plots, which is an indication of the common underlying mechanism of brain circuit shifts from resting states to any other activities (see Figure 8, gambling, motor, relational, and social panel).

4. Discussion

At the heart of many complex systems resides a set of fine-tuned mesoscopic structures whose roles have been linked with complex orchestrations of emergent phenomena. Understanding complex higher-order behaviors arisen at a scale between the mesoscopic (brain regions) and macroscopic (whole-brain) level would set the stage for a more comprehensive understanding of the human brain large-scale functional circuitry. There are two kinds of mesoscopic structures: (i) local/quasilocal (e.g., ground-truth communities) and (ii) non-local such as topological strata of complex networks. In this work, we proposed a TDA formalism to disentangle the higher-order properties of brain sub-circuits (FNs) among different fMRI tasks. The major contributions of our framework on higher-order brain systems over other existing ones [6,39,65,66] are that (i) this framework allows for the study of non-localized properties of an a priori set of localized/quasilocalized sub-networks; (ii) through this innovative mesoscopic kernel proposal, we observed various results that align well with the current knowledge in network neuroscience and also highlighted the resting-state dichotomy of default mode network as well as the role of the limbic system in the process of functional (re)configuration; (iii) we included not only within-task and within-FN scenarios, but also investigated the bi-level analysis that considered both task and FN levels at the same time. The construction of fMRI brain connectivity and Yeo's ROI-to-FN mappings enabled multi-level homological group calculation and corresponding graph-based analysis. With seven different tasks in addition to the resting state, previous studies found that the brain functional reconfiguration in macroscopic (global) level is hard to observe, while different tasks will rather trigger more shifts in the mesoscopic structure (brain functional networks level) [14,67,68].Hence, we organized our framework into five settings: (a) group-averaged global level, (b) group-averaged consolidated level, (c) group-averaged mesoscopic level, (d) individual global level, and (e) individual all-to-REST level with functional network analysis and task analysis. At the first three levels, we conducted the topological data analysis at the group-representative level, which gives a broader view of the homological landscape between tasks and functional networks. When we looked at the individual level (each subject's FCs), we took a different approach from other existing brain connectivity fingerprint frameworks [14,69]. Specifically, in the first step, we used consensus analysis to infer group-level behavior, as opposed to using simple averages. In the first step, we computed the distance measures on an individual basis by using the KL divergence to compare the distribution of individual-level distance. Through this setting, we found that three homological groups provided complementary insights into both task and subject domains. More specifically, the zeroth homology measures the connected components; the first homology measures the two-dimensional hole encapsulated by one-dimensional functional edges; the second homology measures the three-dimensional cavities encapsulated by two-dimensional triangles. These homological groups and their algebraic structures are hypothesized in our paper to characterize topological spaces parameterized by the brain connectivity network.

Noticeably, in the work led by Fox and colleagues [70], the authors suggested that the emotion task may be regulated by the reduced functional activity attenuated by self-referential aspects of such task. In general, "harder" tasks (i.e., relational) require an increasing level of global integration which should reflect through a relatively small number of connected components (smaller Betti number 0). It is worth noting that the motor cortex was identified as the hub of broadcasting transduction [16], which contains brain regions that are critical to broadcast information to other regions of the brain. Compared to the resting state, the absence of cognitive requirement from fMRI tasks, such as the motor task, which employs motor cortex brain regions, modulates global integrative cooperation among brain regions by forming first-order cycles across FNs.Combining both zeroth (connected components) and first homological (graph-theoretical cycles) distance results, we see that there exists a cognitive "switch" taking place at a global level to form connectivities that result in (i) a lesser number of connected components and (ii) more globally integrated FNs as reflected by first-order cycles.

By consolidating the global view of the group-averaged connectome, we found that the H_1 homology displayed stable topological invariants with its consistency in the most distinct pair of tasks as well as pertaining to a clear block diagonal structure on the distance heatmap. Both global and consolidated views displayed significant signals that the resting state and motor task are the most different task pairs [55,56], while they are also the first and second distinct tasks in terms of the average distance (see Figure 4A,B). In this case, a simple observation we can draw from the analysis is that the brain takes some reconfiguration from resting state to other non-motor tasks, and then it requires further shifts in connectivity to get to the motor task. In addition, we further studied the individual-level homological scaffolds and performed group-level consensus voting on the most differentiated pair of tasks over 100 unrelated subjects (see Figure 6B,C). The H_1 and H_2 majority voting results again showed that the motor task is the most distant task from the resting state, and H_1 also has the highest frequency count on the largest count among all three homological groups, indicating that it has the most consistent and robust capability to understand the homological scaffold in brain connectivity topological space.

Noticeably, the strong topological invariant of the H_1 homology between the macroscopic (whole-brain) level with the consolidated (super-graph) level demonstrated the existence of a self-similarity property unraveled by the higher-order properties of the brain functional sub-circuit [71–73]. Regarding the macroscopic level of the brain connectome as the "zoomed-in" representation of the consolidated graph, the overall pattern of the Wasserstein distance between tasks still holds. While both the macroscopic level and consolidated level have the resting-state task and motor task pair as the most differentiated task pair, further information was found by looking at the row in the distance heatmap that involves the resting state task and motor task as all having a high Wasserstein distance, together forming a block pattern that separates the resting-state task as well as the motor task from the other tasks.This phenomenon guarantees the "parcellation-invariant" property of the first homological group on the complex brain system and provides a consistent potential for this topological framework for other higher-order complex network systems [71,73]. In addition, we can also view the Glasser parcellation of 360 nodes and Yeo functional network of seven regions of interests as two different representations with a many-to-one relationship, and thus the robustness between the macroscopic level and consolidated level in the first homology showed great potential for this framework in its consistency across different brain parcellations. Therefore, this homological setup can help learn the brain's functional behavior in a robust and trustworthy manner for clinical exploratory and discovery.

We partitioned the brain connectome with the seven Yeo functional networks as well as a subcortical structure, resulting in eight separate sub-networks. Since the resting state brain connectivity structure is the closest to Yeo's partition, the first assessment that we conducted at the mesoscopic level was to fix the resting-state task and compare the distance between two functional networks. The mesoscopic level analysis captured the

"functional dichotomy" of the default mode network in the resting state by both the most differentiated task pairs as well as the highest average distance (see Figure 5B,C), where default mode is the most dominant network [14,70,74]. Thus, with such versatility, the same framework setup can be used to learn both (re)configuration across tasks, functional networks, and neurological conditions. The brain network studies typically focus on either the within-task configuration or within-network configuration [15,16,65,75,76], and the individual-level functional network partition further revealed patterns in the brain that are shifted between the resting state to other tasks as well as between two functional networks. The individual all-to-rest mesoscopic analysis considered both task and functional network "switches". Such bi-level perspective allows for the investigation of the most distinct functional network pairs in the resting state on their reconfiguration from resting state to other tasks (see Figure 7). While maintaining the bi-level design of the experiments, we flipped the two-level in the all-to-rest task analysis to investigate, from the resting state to each task, how pairs of functional networks are shifted (see Figure 8). The unique patterns in the top five pairs of functional networks also enabled hub identification in the process of the task switch, and closer tasks also displayed similar patterns, indicating that they underwent similar reconfiguration from the resting state. The KL-divergence of two individual-level distance distributions brought additional insights into how shifts between tasks and reconfiguration among two functional networks can be related together in their functional behaviors.

This study has certain limitations. In the consolidation process from the global-level graph, we specifically opted for max normalization to construct the super graph. Since altering the normalization method may potentially modify the inter-connectivity of functional networks, future research could investigate different normalization techniques. For instance, using average connectivity to define the consolidated graph may impact not only the topological structure of the super graph but also its self-similarity properties from the homological kernels. Moreover, not only does the choice of the homological group influence the distance measure between tasks or functional networks, but the graph itself also plays a crucial role. Our experiments were solely conducted on the Glasser parcellation with 374 nodes (360 cortical regions + 14 sub-cortical regions). Exploring alternative parcellations in both brain cortical and subcortical regions ([29,77,78]) and incorporating multiple parcellation scales could offer additional insights into mesoscopic cognitive reconfiguration and its scaling-related properties. Another limitation of this study is that the study was conducted exclusively on healthy subjects, so our findings are limited to healthy conditions. Future studies will address the homological landscape of different neurological or psychiatric disorders as well as neurodegeneration diseases. In this case, we can not only compare across functional networks and different tasks, but we can also investigate how the macroscopic level brain and mesoscopic level functional network configures across different disease statuses (e.g., cognitive normal (CN), mild cognitive impairment (MCI), and Alzheimer's disease (AD).

5. Conclusions and Future Work

In summary, we presented a novel framework that uses persistent homology to characterize brain connectivity in the topological space. Based on the nature of each homological group, we selected different distance measures correspondingly. The zeroth persistent homology is all born at 0 so the Wasserstein distance is not a good fit, but the Haursdorff distance is more appropriate for measuring the 1D distribution of the point cloud. However, the first and second homology are closer to the diagonal in the persistent homology diagram, and thus the Wasserstein distance with partial mapping which serves as a simulation of moving one distribution to another in a geodesic setting would become better in this case. We validated that the first homology gives very consistent and topological invariant findings at different levels of analysis, which offers a scaling invariant perspective. In addition, we find that the framework is capable of capturing signals that are well-studied in the literature, which is reassuring for the validity of the

discoveries, but also discovered additional unique patterns in the brain circuit triggering diverse processes among different fMRI tasks and resting conditions. Future applications could design more brain tasks to study the brain's behavior and (re)configuration for a more complex task sequence or even in continuous time [39,79,80], such that we can explore how different subjects behave differently and how their brain (re)configuration is triggered with the same series of tasks. This could also be extended to study the brain functional trajectory in a cascade sequence of tasks and investigate the dynamic of how those functional sub-circuits are coupled during the process. From a wider perspective, our formalism can be applied, beyond brain connectomics, to study non-localized coordination patterns induced by localized, pre-defined structures stretching across different complex network fibers.

Supplementary Materials: The following supporting information can be downloaded at: https://www.mdpi.com/article/10.3390/math12030455/s1, Figure S1: Persistent diagram of the global, group-averaged connectome; Figure S2: Persistent diagram of the consolidated, group-averaged connectome; Figure S3: Group-Average Homological distances between brain circuits (FNs) in emotion task; Figure S4: Group-Average Homological distances between brain circuits (FNs) in gambling task; Figure S5: Group-Average Homological distances between brain circuits (FNs) in language task; Figure S6: Group-Average Homological distances between brain circuits (FNs) in motion task; Figure S7: Group-Average Homological distances between brain circuits (FNs) in relational task; Figure S8: Group-Average Homological distances between brain circuits (FNs) in social task; Figure S9: Group-Average Homological distances between brain circuits (FNs) at working memory task; Figure S10: Distribution of pairs of functional networks having the highest distance in three homological groups; Figure S11: KL divergence circular plot for 7 fMRI tasks-to-REST with functional network comparison in H0; Figure S12: KL divergence circular plot for 7 fMRI tasks-to-REST with functional network comparison in H2.

Author Contributions: D.D.-T.: Conceptualization; Formal analysis; Investigation; Methodology; Writing original draft. R.K.: Methodology; Investigation; Writing original draft. J.C.: Investigation; Formal Analysis; Visualization; Writing original draft. X.W., S.G., F.H.X., A.D.K., and Y.Z.: Writing—review and editing. J.B.: Visualization. G.P.: Methodology; Writing—review and editing. E.A. and J.G.: Data curation; Writing—review and editing. L.S.: Conceptualization; Formal analysis; Writing original draft; Project Supervision; Funding acquisition. All authors have read and agreed to the published version of the manuscript.

Funding: This work was supported in part by the National Institutes of Health grants RF1 AG068191, R01 AG071470, U01 AG068057, and T32 AG076411, the National Science Foundation grant IIS 1837964, and Office of Naval Research N0001423WX00749.

Data Availability Statement: The data used in this study are freely available on the HCP website (https://www.humanconnectome.org, accessed on 1 September 2021). The release Q3 from the HCP data with resting state and seven fMRI tasks and Glasser parcellation was used, and users must apply for permission to access the data. The code for the homological landscape framework is public at the GitHub repository https://github.com/PennShenLab/Homological_Landscape (updated on 17 January 2024), example code offers analysis at the macroscopic level.

Acknowledgments: Data were provided (in part) by the Human Connectome Project, WU-Minn Consortium (principal investigators: David Van Essen and Kamil Ugurbil; 1U54MH091657) funded by the 16 NIH Institutes and Centers that support the NIH Blueprint for Neuroscience Research; and by the McDonnell Center for Systems Neuroscience at Washington University.

Conflicts of Interest: The authors declare no conflicts of interest.

Abbreviations

The following abbreviations are used in this manuscript:

TDA	Topological data analysis
FCs	Functional connectomes
FN	Functional network
VIS	Visual
SM	SomatoMotor
DA	Dorsal atention
VA	Ventral attention
LIM	Limbic
FP	Frontopatietal
DMN	Default mode network
SUBC	Sub-cortical regions
KL divergence	Kullback–Leibler divergence

References

1. Battiston, F.; Amico, E.; Barrat, A.; Bianconi, G.; Ferraz de Arruda, G.; Franceschiello, B.; Iacopini, I.; Kéfi, S.; Latora, V.; Moreno, Y.; et al. The physics of higher-order interactions in complex systems. *Nat. Phys.* **2021**, *17*, 1093–1098. [CrossRef]
2. Giusti, C.; Pastalkova, E.; Curto, C.; Itskov, V. Clique topology reveals intrinsic geometric structure in neural correlations. *Proc. Natl. Acad. Sci. USA* **2015**, *112*, 13455–13460. [CrossRef]
3. Giusti, C.; Ghrist, R.; Bassett, D.S. Two's company, three (or more) is a simplex. *J. Comput. Neurosci.* **2016**, *41*, 1–14. [CrossRef] [PubMed]
4. Yu, S.; Yang, H.; Nakahara, H.; Santos, G.S.; Nikolić, D.; Plenz, D. Higher-order interactions characterized in cortical activity. *J. Neurosci.* **2011**, *31*, 17514–17526. [CrossRef]
5. Schneidman, E.; Berry, M.J.; Segev, R.; Bialek, W. Weak pairwise correlations imply strongly correlated network states in a neural population. *Nature* **2006**, *440*, 1007–1012. [CrossRef]
6. Santoro, A.; Battiston, F.; Petri, G.; Amico, E. Higher-order organization of multivariate time series. *Nat. Phys.* **2023**, *19*, 221–229. [CrossRef]
7. Bassett, D.S.; Gazzaniga, M.S. Understanding complexity in the human brain. *Trends Cognit. Sci.* **2011**, *15*, 200–209. [CrossRef] [PubMed]
8. Meunier, D.; Lambiotte, R.; Fornito, A.; Ersche, K.; Bullmore, E.T. Hierarchical modularity in human brain functional networks. *Front. Neuroinform.* **2009**, *3*, 37. [CrossRef]
9. Bullmore, E.; Sporns, O. Complex brain networks: Graph theoretical analysis of structural and functional systems. *Nat. Rev. Neurosci.* **2009**, *10*, 186–198. [CrossRef] [PubMed]
10. Sporns, O.; Betzel, R.F. Modular brain networks. *Annu. Rev. Psychol.* **2016**, *67*, 613–640. [CrossRef]
11. Abbe, E. Community detection and stochastic block models: Recent developments. *J. Mach. Learn. Res.* **2017**, *18*, 6446–6531.
12. Fortunato, S. Community detection in graphs. *Phys. Rep.* **2010**, *486*, 75–174. [CrossRef]
13. Fortunato, S.; Hric, D. Community detection in networks: A user guide. *Phys. Rep.* **2016**, *659*, 1–44. [CrossRef]
14. Duong-Tran, D.; Kausar, A.; Amico, E.; Corominas-Murtra, B.; Dzemidzic, M.; Kareken, D.; Ventresca, M.; Goñi, J. A morphospace of functional configuration to assess configural breadth based on brain functional networks. *Netw. Neurosci.* **2021**, *5*, 666–688. [CrossRef] [PubMed]
15. Bassett, D.S.; Wymbs, N.F.; Porter, M.A.; Mucha, P.J.; Carlson, J.M.; Grafton, S.T. Dynamic reconfiguration of human brain networks during learning. *Proc. Natl. Acad. Sci. USA* **2011**, *108*, 7641–7646. [CrossRef] [PubMed]
16. Amico, E.; Arenas, A.; Goñi, J. Centralized and distributed cognitive task processing in the human connectome. *Netw. Neurosci.* **2019**, *3*, 455–474. [CrossRef]
17. Yeo, B.T.; Krienen, F.M.; Sepulcre, J.; Sabuncu, M.R.; Lashkari, D.; Hollinshead, M.; Roffman, J.L.; Smoller, J.W.; Zöllei, L.; Polimeni, J.R.; et al. The organization of the human cerebral cortex estimated by intrinsic functional connectivity. *J. Neurophysiol.* **2011**, *106*, 1125–1165.
18. Bryce, N.; Flournoy, J.; Moreira, J.F.G.; Rosen, M.L.; Sambook, K.A.; Mair, P.; McLaughlin, K.A. Brain parcellation selection: An overlooked decision point with meaningful effects on individual differences in resting-state functional connectivity. *NeuroImage* **2021**, *243*, 118487. [CrossRef]
19. Lopez, K.C.; Kandala, S.; Marek, S.; Barch, D.M. Development of network topology and functional connectivity of the prefrontal cortex. *Cereb. Cortex* **2020**, *30*, 2489–2505. [CrossRef]
20. Murphy, A.C.; Bertolero, M.A.; Papadopoulos, L.; Lydon-Staley, D.M.; Bassett, D.S. Multimodal network dynamics underpinning working memory. *Nat. Commun.* **2020**, *11*, 1–13. [CrossRef]
21. Jalbrzikowski, M.; Liu, F.; Foran, W.; Calabro, F.J.; Roeder, K.; Devlin, B.; Luna, B. Cognitive and default mode networks support developmental stability in functional connectome fingerprinting through adolescence. *bioRxiv* **2019**. [CrossRef]

22. Satterthwaite, T.D.; Elliott, M.A.; Gerraty, R.T.; Ruparel, K.; Loughead, J.; Calkins, M.E.; Eickhoff, S.B.; Hakonarson, H.; Gur, R.C.; Gur, R.E.; et al. An improved framework for confound regression and filtering for control of motion artifact in the preprocessing of resting-state functional connectivity data. *Neuroimage* **2013**, *64*, 240–256. [CrossRef]
23. Fan, J.; Tso, I.F.; Maixner, D.F.; Abagis, T.; Hernandez-Garcia, L.; Taylor, S.F. Segregation of salience network predicts treatment response of depression to repetitive transcranial magnetic stimulation. *NeuroImage Clin.* **2019**, *22*, 101719. [CrossRef] [PubMed]
24. Lydon-Staley, D.; Kuehner, C.; Zamoscik, V.; Huffziger, S.; Kirsch, P.; Bassett, D. Repetitive negative thinking in daily life and functional connectivity among default mode, fronto-parietal, and salience networks. *Transl. Psychiatry* **2019**, *9*, 1–12. [CrossRef]
25. Xu, F.; Garai, S.; Duong-Tran, D.; Saykin, A.J.; Zhao, Y.; Shen, L. Consistency of Graph Theoretical Measurements of Alzheimer's Disease Fiber Density Connectomes Across Multiple Parcellation Scales. In Proceedings of the 2022 IEEE International Conference on Bioinformatics and Biomedicine (BIBM), Las Vegas, NV, USA, 6–8 December 2022; pp. 1323–1328.
26. Power, J.D.; Cohen, A.L.; Nelson, S.M.; Wig, G.S.; Barnes, K.A.; Church, J.A.; Vogel, A.C.; Laumann, T.O.; Miezin, F.M.; Schlaggar, B.L.; et al. Functional network organization of the human brain. *Neuron* **2011**, *72*, 665–678. [CrossRef] [PubMed]
27. Glasser, M.F.; Coalson, T.S.; Robinson, E.C.; Hacker, C.D.; Harwell, J.; Yacoub, E.; Ugurbil, K.; Andersson, J.; Beckmann, C.F.; Jenkinson, M.; et al. A multi-modal parcellation of human cerebral cortex. *Nature* **2016**, *536*, 171–178. [CrossRef]
28. Gordon, E.M.; Laumann, T.O.; Adeyemo, B.; Huckins, J.F.; Kelley, W.M.; Petersen, S.E. Generation and evaluation of a cortical area parcellation from resting-state correlations. *Cereb. Cortex* **2016**, *26*, 288–303. [CrossRef]
29. Schaefer, A.; Kong, R.; Gordon, E.M.; Laumann, T.O.; Zuo, X.N.; Holmes, A.J.; Eickhoff, S.B.; Yeo, B.T. Local-global parcellation of the human cerebral cortex from intrinsic functional connectivity MRI. *Cereb. Cortex* **2018**, *28*, 3095–3114. [CrossRef]
30. Schneider, C.M.; Moreira, A.A.; Andrade, J.S.; Havlin, S.; Herrmann, H.J. Mitigation of malicious attacks on networks. *Proc. Natl. Acad. Sci. USA* **2011**, *108*, 3838–3841. [CrossRef] [PubMed]
31. Gardner, R.J.; Hermansen, E.; Pachitariu, M.; Burak, Y.; Baas, N.A.; Dunn, B.A.; Moser, M.B.; Moser, E.I. Toroidal topology of population activity in grid cells. *Nature* **2022**, *602*, 123–128. [CrossRef]
32. Saleh, N.A.; Mahmoud, M.A.; Jones-Farmer, L.A.; Zwetsloot, I.; Woodall, W.H. Another look at the EWMA control chart with estimated parameters. *J. Qual. Technol.* **2015**, *47*, 363. [CrossRef]
33. Salehi, M.; Greene, A.S.; Karbasi, A.; Shen, X.; Scheinost, D.; Constable, R.T. There is no single functional atlas even for a single individual: Parcellation of the human brain is state dependent. *bioRxiv* **2018**. [CrossRef]
34. Glasser, M.F.; Sotiropoulos, S.N.; Wilson, J.A.; Coalson, T.S.; Fischl, B.; Andersson, J.L.; Xu, J.; Jbabdi, S.; Webster, M.; Polimeni, J.R.; et al. The minimal preprocessing pipelines for the Human Connectome Project. *Neuroimage* **2013**, *80*, 105–124. [CrossRef] [PubMed]
35. Carlsson, G. Topological pattern recognition for point cloud data. *Acta Numer.* **2014**, *23*, 289–368. [CrossRef]
36. Shine, J.M.; Bissett, P.G.; Bell, P.T.; Koyejo, O.; Balsters, J.H.; Gorgolewski, K.J.; Moodie, C.A.; Poldrack, R.A. The dynamics of functional brain networks: Integrated network states during cognitive task performance. *Neuron* **2016**, *92*, 544–554. [CrossRef]
37. Shine, J.M.; Poldrack, R.A. Principles of dynamic network reconfiguration across diverse brain states. *NeuroImage* **2017**, *80*, 396–405. [CrossRef]
38. Shine, J.; Breakspear, M.; Bell, P.; Ehgoetz, K.M.; Shine, R.; Koyejo, O.; Sporns, O.; Poldrack, R. The dynamic basis of cognition: An integrative core under the control of the ascending neuromodulatory system. *bioRxiv* **2018**. [CrossRef]
39. Shine, J.M.; Breakspear, M.; Bell, P.; Martens, K.E.; Shine, R.; Koyejo, O.; Sporns, O.; Poldrack, R. Human cognition involves the dynamic integration of neural activity and neuromodulatory systems. *Nat. Neurosci.* **2019**, *22*, 89–96. [CrossRef]
40. Duong-Tran, D. On Geometric and Algebraic Properties of Human Brain Functional Networks. Ph.D. Thesis, Purdue University Graduate School, West Lafayette, Indiana, 2022.
41. Abbe, E.; Sandon, C. Proof of the achievability conjectures for the general stochastic block model. *Commun. Pure Appl. Math.* **2018**, *71*, 1334–1406. [CrossRef]
42. Edelsbrunner, H.; Harer, J. *Computational Topology: An Introduction*; American Mathematical Society: Providence, RI, USA, 2010.
43. Petri, G.; Expert, P.; Turkheimer, F.; Carhart-Harris, R.; Nutt, D.; Hellyer, P.J.; Vaccarino, F. Homological scaffolds of brain functional networks. *J. R. Soc. Interface* **2014**, *11*, 20140873. [CrossRef]
44. Fornito, A.; Zalesky, A.; Breakspear, M. The connectomics of brain disorders. *Nat. Rev. Neurosci.* **2015**, *16*, 159. [CrossRef]
45. Duong-Tran, D.; Amico, E.; Corominas-Murtra, B.; Abbas, K.; Dzemidzic, M.; Kareken, D.; Ventresca, M.; Goñi, J. A morphospace framework to assess configural breadth based on brain functional networks. *arXiv* **2019**, arXiv:1901.10962.
46. Betzel, R.F.; Medaglia, J.D.; Bassett, D.S. Diversity of meso-scale architecture in human and non-human connectomes. *Nat. Commun.* **2018**, *9*, 346. [CrossRef] [PubMed]
47. Fornito, A.; Zalesky, A.; Bullmore, E. *Fundamentals of Brain Network Analysis*; Academic Press: Cambridge, MA, USA, 2016.
48. Van Essen, D.C.; Ugurbil, K.; Auerbach, E.; Barch, D.; Behrens, T.; Bucholz, R.; Chang, A.; Chen, L.; Corbetta, M.; Curtiss, S.W.; et al. The Human Connectome Project: A data acquisition perspective. *Neuroimage* **2012**, *62*, 2222–2231. [CrossRef] [PubMed]
49. Van Essen, D.C.; Smith, S.M.; Barch, D.M.; Behrens, T.E.; Yacoub, E.; Ugurbil, K.; Consortium, W.M.H. The WU-Minn human connectome project: An overview. *Neuroimage* **2013**, *80*, 62–79. [CrossRef]
50. Barch, D.M.; Burgess, G.C.; Harms, M.P.; Petersen, S.E.; Schlaggar, B.L.; Corbetta, M.; Glasser, M.F.; Curtiss, S.; Dixit, S.; Feldt, C.; et al. Function in the human connectome: Task-fMRI and individual differences in behavior. *Neuroimage* **2013**, *80*, 169–189. [CrossRef]

51. Smith, S.M.; Beckmann, C.F.; Andersson, J.; Auerbach, E.J.; Bijsterbosch, J.; Douaud, G.; Duff, E.; Feinberg, D.A.; Griffanti, L.; Harms, M.P.; et al. Resting-state fMRI in the human connectome project. *Neuroimage* **2013**, *80*, 144–168. [CrossRef]
52. Amico, E.; Goñi, J. The quest for identifiability in human functional connectomes. *Sci. Rep.* **2018**, *8*, 8254. [CrossRef]
53. Amico, E.; Goñi, J. Mapping hybrid functional-structural connectivity traits in the human connectome. *Netw. Neurosci.* **2018**, *2*, 306–322. [CrossRef]
54. Lashkari, D.; Vul, E.; Kanwisher, N.; Golland, P. Discovering structure in the space of fMRI selectivity profiles. *Neuroimage* **2010**, *50*, 1085–1098. [CrossRef] [PubMed]
55. Di, X.; Gohel, S.; Kim, E.H.; Biswal, B.B. Task vs. rest—Different network configurations between the coactivation and the resting-state brain networks. *Front. Hum. Neurosci.* **2013**, *7*, 493. [CrossRef]
56. Huang, J. Greater brain activity during the resting state and the control of activation during the performance of tasks. *Sci. Rep.* **2019**, *9*, 5027. [CrossRef]
57. Raichle, M.E.; MacLeod, A.M.; Snyder, A.Z.; Powers, W.J.; Gusnard, D.A.; Shulman, G.L. A default mode of brain function. *Proc. Natl. Acad. Sci. USA* **2001**, *98*, 676–682. [CrossRef] [PubMed]
58. Buckner, R.L.; Andrews-Hanna, J.R.; Schacter, D.L. The brain's default network: Anatomy, function, and relevance to disease. *Ann. N. Y. Acad. Sci.* **2008**, *1124*, 1–38. [CrossRef] [PubMed]
59. Fransson, P. Spontaneous low-frequency BOLD signal fluctuations: An fMRI investigation of the resting-state default mode of brain function hypothesis. *Hum. Brain Map.* **2005**, *26*, 15–29. [CrossRef] [PubMed]
60. Zhong, X.; Pu, W.; Yao, S. Functional alterations of fronto-limbic circuit and default mode network systems in first-episode, drug-naïve patients with major depressive disorder: A meta-analysis of resting-state fMRI data. *J. Affect. Disord.* **2016**, *206*, 280–286. [CrossRef] [PubMed]
61. Catani, M.; Dell'Acqua, F.; De Schotten, M.T. A revised limbic system model for memory, emotion and behaviour. *Neurosci. Biobehav. Rev.* **2013**, *37*, 1724–1737. [CrossRef] [PubMed]
62. Roxo, M.R.; Franceschini, P.R.; Zubaran, C.; Kleber, F.D.; Sander, J.W. The limbic system conception and its historical evolution. *Sci. World J.* **2011**, *11*, 2427–2440. [CrossRef] [PubMed]
63. Hariri, A.R.; Bookheimer, S.Y.; Mazziotta, J.C. Modulating emotional responses: Effects of a neocortical network on the limbic system. *Neuroreport* **2000**, *11*, 43–48. [CrossRef]
64. Kullback, S. *Information Theory and Statistics*; Courier Corporation: Mineola, NY, USA, 1997.
65. Schultz, D.H.; Cole, M.W. Higher intelligence is associated with less task-related brain network reconfiguration. *J. Neurosci.* **2016**, *36*, 8551–8561. [CrossRef]
66. Amico, E.; Abbas, K.; Duong-Tran, D.A.; Tipnis, U.; Rajapandian, M.; Chumin, E.; Ventresca, M.; Harezlak, J.; Goñi, J. Toward an information theoretical description of communication in brain networks. *Netw. Neurosci.* **2021**, *5*, 646–665. [CrossRef] [PubMed]
67. Cole, M.W.; Bassett, D.S.; Power, J.D.; Braver, T.S.; Petersen, S.E. Intrinsic and task-evoked network architectures of the human brain. *Neuron* **2014**, *83*, 238–251. [CrossRef]
68. Mohr, H.; Wolfensteller, U.; Betzel, R.F.; Mišić, B.; Sporns, O.; Richiardi, J.; Ruge, H. Integration and segregation of large-scale brain networks during short-term task automatization. *Nat. Commun.* **2016**, *7*, 13217. [CrossRef]
69. Abbas, K.; Liu, M.; Venkatesh, M.; Amico, E.; Kaplan, A.D.; Ventresca, M.; Pessoa, L.; Harezlak, J.; Goñi, J. Geodesic distance on optimally regularized functional connectomes uncovers individual fingerprints. *Brain Connect.* **2021**, *11*, 333–348. [CrossRef]
70. Fox, M.D.; Snyder, A.Z.; Vincent, J.L.; Corbetta, M.; Van Essen, D.C.; Raichle, M.E. The human brain is intrinsically organized into dynamic, anticorrelated functional networks. *Proc. Natl. Acad. Sci. USA* **2005**, *102*, 9673–9678. [CrossRef] [PubMed]
71. Song, C.; Havlin, S.; Makse, H.A. Self-similarity of complex networks. *Nature* **2005**, *433*, 392–395. [CrossRef] [PubMed]
72. Song, C.; Havlin, S.; Makse, H.A. Origins of fractality in the growth of complex networks. *Nat. Phys.* **2006**, *2*, 275–281. [CrossRef]
73. Singh, S.S.; Khundrakpam, B.; Reid, A.T.; Lewis, J.D.; Evans, A.C.; Ishrat, R.; Sharma, B.I.; Singh, R.B. Scaling in topological properties of brain networks. *Sci. Rep.* **2016**, *6*, 24926. [CrossRef] [PubMed]
74. Greicius, M.D.; Krasnow, B.; Reiss, A.L.; Menon, V. Functional connectivity in the resting brain: A network analysis of the default mode hypothesis. *Proc. Natl. Acad. Sci. USA* **2003**, *100*, 253–258. [CrossRef]
75. Betzel, R.F.; Satterthwaite, T.D.; Gold, J.I.; Bassett, D.S. Positive affect, surprise, and fatigue are correlates of network flexibility. *Sci. Rep.* **2017**, *7*, 520. [CrossRef]
76. Bertolero, M.A.; Yeo, B.T.; D'Esposito, M. The modular and integrative functional architecture of the human brain. *Proc. Natl. Acad. Sci. USA* **2015**, *112*, E6798–E6807. [CrossRef]
77. Tian, Y.; Margulies, D.S.; Breakspear, M.; Zalesky, A. Hierarchical organization of the human subcortex unveiled with functional connectivity gradients. *bioRxiv* **2018**. [CrossRef]
78. Revell, A.Y.; Silva, A.B.; Arnold, T.C.; Stein, J.M.; Das, S.R.; Shinohara, R.T.; Bassett, D.S.; Litt, B.; Davis, K.A. A framework For brain atlases: Lessons from seizure dynamics. *Neuroimage* **2022**, *254*, 118986. [CrossRef] [PubMed]

79. Barnes, A.; Bullmore, E.T.; Suckling, J. Endogenous human brain dynamics recover slowly following cognitive effort. *PLoS ONE* **2009**, *4*, e6626. [CrossRef] [PubMed]
80. Douw, L.; Wakeman, D.G.; Tanaka, N.; Liu, H.; Stufflebeam, S.M. State-dependent variability of dynamic functional connectivity between frontoparietal and default networks relates to cognitive flexibility. *Neuroscience* **2016**, *339*, 12–21. [CrossRef] [PubMed]

Disclaimer/Publisher's Note: The statements, opinions and data contained in all publications are solely those of the individual author(s) and contributor(s) and not of MDPI and/or the editor(s). MDPI and/or the editor(s) disclaim responsibility for any injury to people or property resulting from any ideas, methods, instructions or products referred to in the content.